Available online at www.sciencedirect.com
ScienceDirect
Journal of the European Ceramic Society 30 (2010) 2691–2697
www.elsevier.com/locate/jeurceramsoc

Investigation of ceramic boron nitride by terahertz time-domain spectroscopy

Mira Naftaly [a,*], Jon Leist [b], Richard Dudley [a]

[a] National Physical Laboratory, Hampton Road, Teddington, TW11 0LW, UK
[b] Momentive Performance Materials, Inc., 22557 West Lunn Road, Strongsville, OH 44070, USA

Received 10 February 2010; accepted 26 April 2010
Available online 21 May 2010

Abstract

Four grades of hexagonal boron nitride are investigated by terahertz time-domain spectroscopy. The refractive indices and loss coefficients at terahertz frequencies are measured and are related to aspects of material fabrication and properties.

Keywords: Boron nitride; Terahertz spectroscopy; Optical properties; Porosity

1. Introduction

Boron nitride is a synthetic ceramic with three possible morphologies analogous to the polymorphs of carbon. Two hexagonal forms exist: one of lower density (2.27 g/cm^3) and displaying a layered graphite structure (*h*-BN)[1,2]; the other of higher density (3.48 g/cm^3) and displaying a wurtzite structure (*w*-BN).[2,3] A diamond-like form with cubic zinc-blende structure (*c*-BN) can also be generated under high temperature and pressure.[2,4] For the purposes of this paper, the term 'BN' will refer to the low-density hexagonal form (*h*-BN).

Hexagonal boron nitride is comprised of $(BN)_3$ rings, with very strong intra-layer bonding and weak van der Waals bonding between layers (Fig. 1a).[5] This structure enables phonon conduction within layers, explaining the high thermal conductivities of both graphite and BN. The similarities end there, as graphite is a black metallic conductor and BN is white insulator. These differences find their origin in the interlayer arrangement of C atoms in graphite versus B and N atoms in BN. Carbon atoms in adjacent layers of graphite align with one another, and their π-orbitals combine in such a way as to form conduction and valence bands. The interlayer B and N atoms of BN are staggered in their arrangement, preventing π-orbital overlap (Fig. 1a). As a result, electrons in *h*-BN are localized and electrical conduction cannot occur.

The unique intra-layer and interlayer bonding structure of BN is the source of its versatility for a number of diverse applications. The van der Waals bonding between layers and the strong covalent bonding within layers allows adjacent layers to slide over one another with low interaction. For this reason, BN powder is an important friction modifier and noise reducer in brake linings and other friction materials,[6] a wear and weld prevention additive for lubricating oils and greases,[7] and a lubricious sensory enhancer in personal care products.[8] The strong, intra-layer covalent bonding and low surface activity of the basal plane allow BN powder to be used in non-wetting refractory coatings for molten metal processing,[9] as well as release coatings for hot metal forging. The electrical insulating character and thermal conductivity of BN make it valuable as an additive in thermal interface greases and pads for cooling electronic devices.[10] Addition of BN powder to matrices, be they metal, ceramic, or polymer, usually results in a weakening of the matrix at a critical concentration. This aspect of BN is used in thermally sprayed abradable coatings for aircraft engine housings, where coatings comprised of BN and metals allow turbine blades to smear the housing coating and maintain a close tolerance between the blade tip and the housing, which translates into improved engine efficiencies.[11] The thermal conductivity and inert nature of BN powder also improve thermal shock resistance and machinability of metal and ceramic matrices to which it is added.[12]

Hot-pressing methods have been developed to achieve nearly full-density shapes comprised of BN, as well as BN composites with other ceramic materials. A wide variety of applications exist

* Corresponding author.
E-mail address: mira.naftaly@npl.co.uk (M. Naftaly).

0955-2219/$ – see front matter.
doi:10.1016/j.jeurceramsoc.2010.04.040

for these shapes, including high temperature electrical insulators for industrial and semiconductor processes, crucibles and furniture for molten metals and glass processing, inert setter plates for ceramic sintering, nozzles for metal powder generation, and furniture for epitaxial device growth. With such a diverse array of applications for BN powders and shapes, there exists a need to quantify many different properties. It is important to understand the effect of microstructure and chemistry on the end use of the material, as well as to control these properties in the manufacturing process.

A comprehensive list of properties of *h*-BN is available at[2] http://www.ioffe.rssi.ru/SVA/NSM/Semicond/BN/basic.html. Although *h*-BN has good transparency in the far-infrared, there is little published data,[1,2,13–15] and no attempt has been made to relate far-infrared transmission to aspects of material properties.

In this paper we investigate four grades of *h*-BN using THz time-domain spectroscopy. The variations in the refractive index and loss are discussed in relation to material fabrication and structure. The utility of *h*-BN as an optical material at THz frequencies is also explored.

2. Material fabrication

Due to the low surface energy of the *c*-plane (Fig. 1a), BN does not self-sinter.[16] High-density freestanding shapes are achievable by hot-pressing submicron, turbostratic BN in the presence of a binder phase under temperatures approaching 2000 °C and pressures up to 2000 psi. Turbostratic BN is analogous to turbostratic graphite, where adjacent layers are offset rotationally with respect to the *c*-axis. The selection of binder phase is dictated by the final application requirements. High purity grades of hot pressed BN are also available, with the binder phase leached from the shape after it is generated. The grades described below – designated as HBN, HBR, HBC and HBT – are manufactured by Momentive Performance Materials and are representative of commercially available forms of hot pressed boron nitride.

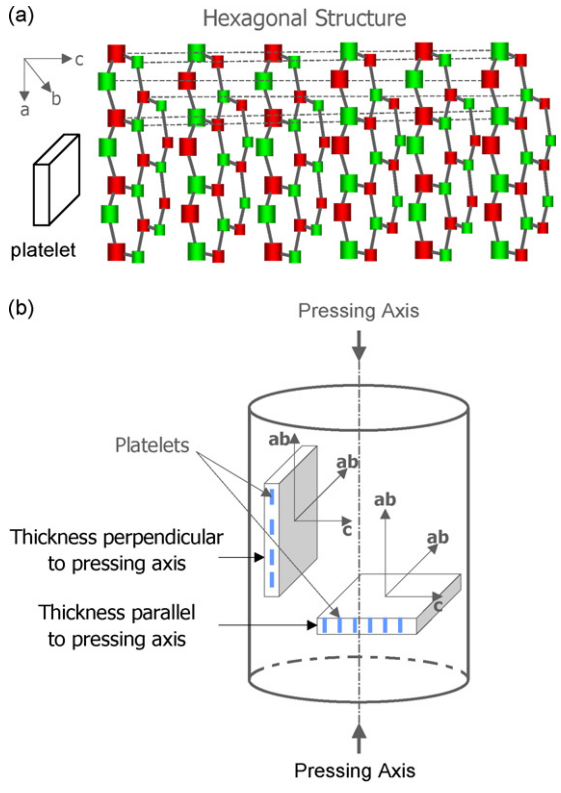

Fig. 1. (a) A diagram of the pressing process and sample orientation showing the sample planes. (b) A schematic representation of the BN crystal structure showing sample planes in relation to crystal growth.

2.1. Grade HBN

Boric oxide (B_2O_3) constitutes the binder phase for grade HBN. Boric oxide is a hard and moderate-temperature inorganic binder, with a nominal melting point of 550 °C. The molten phase is also known to mediate growth and refinement of turbostratic BN. A peculiarity of the hot-pressing of BN is that individual grains or platelets tend to 'stand up proud' and align themselves along the direction of the pressing axis. In other words, there is a strong tendency for the normal to the *c*-plane in each platelet to assume a preferential orientation perpendicular to the pressing axis (Fig. 1b), producing a relatively narrow distribution of orientations around perfect alignment. This preferential orientation is also reflected in the physical properties of grade HBN: data must be reported with respect to the pressing axis, and orientation must be specified when designing parts based on this grade. Upon cooling, the boric oxide phase in the resulting cylindrical 'plug' forms a glassy phase. Due to the low surface activity of the basal plane in BN, boric oxide is preferentially segregated at the edges of platelets in the pressed plug. As boric oxide is known to react readily with moisture to form boric acid, the HBN grade is used when moisture resistance and thermal shock are not a concern.

2.2. Grade HBC

Some applications require a material of high purity, less likely to release volatile components. Grade HBC is manufactured by removing the boric oxide binder phase from the hot pressed BN shape. The purity gain is offset by a loss of mechanical strength and an increase in porosity. However, the resulting material is also more resistant to moisture and thermal shock. Orientation effects of the original hot pressed BN material are maintained.

2.3. Grade HBT

Grade HBT is an economical high purity material similar to grade HBC. The binder phase in this material is removed by a different method from that used to manufacture HBC. Mechanical strength suffers and porosity increases to achieve the cost benefit. Again, the absence of boric oxide phase makes the material more resistant to moisture and thermal shock. Orientation effects of the starting hot pressed BN material are maintained.

2.4. Grade HBR

Grade HBR was developed for applications where higher mechanical strength, higher temperatures, and moisture resistance are important. The binder phase in this material is calcium borate ($Ca_3(BO_3)_2$), an inorganic material with a nominal melting point of 1150 °C. Calcium borate is not water-soluble, so moisture sensitivity is not an issue. The hot-pressing process for this grade is similar to that for grade HBN, and it displays the same orientation effects.

2.5. Sample geometry and orientation

Fig. 1a is a schematic representation of the material structure indicating the sample planes; whilst Fig. 1b is a diagram of the pressing geometry and sample orientation. As explained above, the pressed plug is formed as an array of standing platelets, which assume a preferential orientation with respect to the pressing direction such that their *c*-plane is parallel to the pressing axis. Each platelet consists of hexagonal crystals aligned with their *ab*-plane lying in the plane of the platelet. Materials having hexagonal crystal structure are expected to be optically anisotropic, the resulting birefringence being such that the extraordinary ray lies in the *ab*-plane and the ordinary ray is aligned with the *c*-axis.

In carrying out transmission measurements, samples were positioned so that the linearly polarised THz beam had a near-zero angle of incidence on the sample face and propagated through the thickness of the sample. In the samples cut perpendicular to the pressing axis, the beam travelled along the *c*-axis, so that both polarisations lay in the *ab*-plane. In samples cut parallel to the pressing axis, the beam traversed the thickness of the platelets, so that s-polarisation (electric field perpendicular to the plane of incidence) lay in the *ab*-plane while p-polarisation (electric field parallel to the plane of incidence) was parallel to the *c*-axis. Therefore perpendicular-cut samples are expected to be isotropic, while parallel-cut samples are expected to be birefringent and possibly dichroic.

Table 1 summarises the composition and properties of the four boron nitride grades. The porosity was calculated from the measured weight of a given volume of the material and the known density of crystalline BN (2.18 g/cm^3 [2]), including binders, if applicable. Any weight deficit was assumed to be attributable to porosity.

Sample plates for each grade were fabricated with dimensions of 30 mm diameter and two thicknesses, 2.5 mm and 5 mm. One set of samples was cut with their thickness parallel to the pressing axis, resulting in the face being composed of edges of *c*-planes.

Table 1
Properties of different grades of boron nitride.

	HBN	HBR	HBC	HBT
BN content	>95%	>94%	>99%	>99%
Binder	B_2O_3	$Ca_3(BO_3)_2$	None	None
Density (g/cm^3)	2.10	2.00	1.95	1.75
Porosity (%)	7	11	13	22

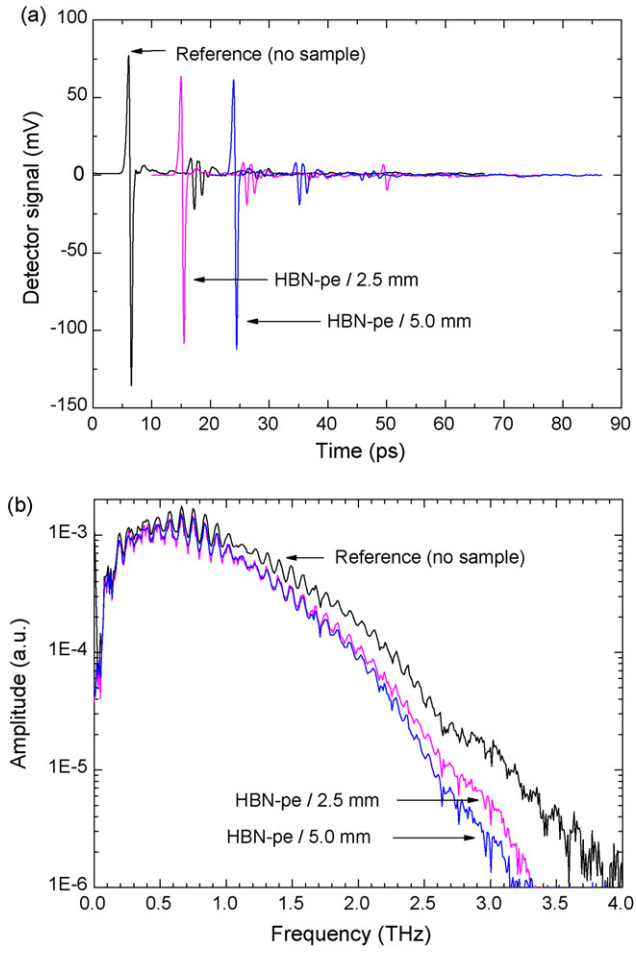

Fig. 2. (a) Time-domain traces of the THz reference pulse and pulses transmitted through HBN perpendicular-cut samples of 2.5 mm and 5 mm thickness. (b) THz spectra of the same calculated by applying Fast Fourier Transform (FFT).

Another set of samples was cut with their thickness perpendicular to pressing axis, resulting in the face being composed of *c*-planes.

3. Experimental

The THz time-domain spectrometer (TDS) used a standard configuration[17] incorporating a femtosecond laser, four off-axis parabolic mirrors, a biased GaAs emitter, and electro-optic detection with a ZnTe crystal and balanced photodiodes. The maximum dynamic range of the system was 5000 in amplitude, and the frequency resolution in the experiments was 7.5 GHz. The samples were placed in the collimated part of the THz beam, which had a diameter of 25 mm and was vertically polarised. Measurements were carried out in dry air in order to eliminate water absorption lines from the recorded spectra. The amplitude and phase of the THz signal as a function of frequency are obtained from the measured time-domain data of THz electric field by applying the Fourier Transform using a standard FFT application (OriginPro 8). Fig. 2a and b shows an example of time-domain data and the resultant spectra, respectively. Loss coefficients (α) and refractive indices (n) of the samples were measured by comparing THz transmission through two different

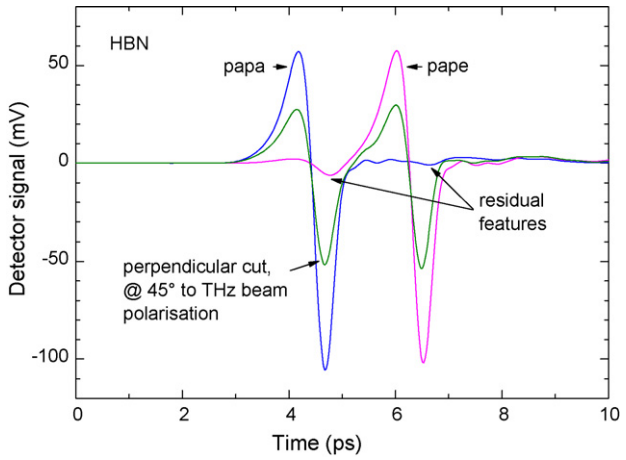

Fig. 3. Time-domain traces of the THz pulses transmitted through the HBN sample of 5 mm thickness cut parallel to the pressing axis; *papa* = aligned parallel to the THz beam polarisation; *pape* = aligned perpendicular to the THz beam polarisation.

thicknesses of the sample material, and were calculated from the transmitted spectra by using the equations[17]:

$$\alpha(\nu) = -\frac{2}{d_1 - d_2} \ln\left[\frac{E_2(\nu)}{E_1(\nu)}\right] \quad (1)$$

$$n(\nu) = 1 + \frac{c\,[\phi_2(\nu) - \phi_1(\nu)]}{2\pi\nu(d_1 - d_2)} \quad (2)$$

where $E_{1,2}(\nu)$ and $\phi_{1,2}(\nu)$ are the amplitude and phase of the THz field at the frequency ν, and $d_{1,2}$ are the sample thicknesses. Loss coefficients $\alpha(\nu)$ combine contributions from absorption and scattering losses.

The axis directions of the perpendicular-cut samples were determined by observing the time-domain trace of the transmitted THz beam. The sample was positioned in the beam, and was rotated so as to obtain a single-peak trace at one of two delay positions, as shown in Fig. 3. Particular attention was given to minimising the residual features of the other trace. This is because the absence of such features signals good alignment of the THz beam polarisation to the *c*-axis, either parallel (*papa*) or orthogonal (*pape*). However, as seen in Fig. 3, it was not possible to eliminate these residues completely, indicating an imperfect mutual alignment of the platelets in the sample.

4. Results

The refractive indices and loss coefficients of the four *h*-BN grades studied are presented in Fig. 4 and summarised in Table 2. The results may be compared with those in Ref. [13], wherein grades A and HP correspond, respectively, to HBN and HBR. The two sets of results are generally similar, although the values of n_o in the present work are somewhat higher.

All four grades are seen to be birefringent, as expected, with negative birefringence varying from −0.11 to −0.19. Grades HBC, HBN and HBR are weakly dichroic, whilst HBT has significant positive dichroism.

It is not entirely clear what is the origin of oscillations at low frequencies in perpendicular-cut samples. It appears likely that they are artefacts of FFT caused by imperfect alignment of the BN platelets with the pressing axis, observed as small residual features in the time-domain trace (see Fig. 3). The residual features arise because a small extraordinary component accompanies the ordinary beam, and vice versa. The presence of two time-domain peaks, corresponding to two independent spectra generated, respectively, by the ordinary and the extraordinary beams, is translated by the FFT into oscillations in the combined single calculated spectrum.

The values of the THz refractive index and loss coefficient for *pe* and *papa* sample orientations are expected to be equal within the measurement error, since both relate to propagation along the extraordinary axis. The small observed differences may be caused by the imperfect alignment of the BN platelets with the pressing axis (see Fig. 3). The slight increase of the refractive index with frequency is attributed to the tail of the lowest phonon resonance at 23 THz.[18]

In comparing the values for different grades, it may be expected that the refractive index will decrease linearly with increasing porosity, since less material lies in the optical path. Fig. 5 depicts the relationship. The most notable feature of Fig. 5 is that the extraordinary refractive index decreases with porosity, as expected, but the ordinary index does not. This supports the view that porosity in these materials is located predominantly at the edges of the *c*-planes, rather than at the *c*-plane faces which have low surface energy. The extraordinary ray is polarised in the plane of the platelets, therefore experiencing an effective refractive index which is modified (reduced) by the interstices between the platelet edges. The ordinary ray, which is polarised transversely to the platelets, would be similarly affected by interstices between platelet layers. The absence of such effect indicates the absence of porosity between platelet faces.

The intercept at zero porosity of the ordinary refractive index is 2.12, which is in good agreement with the single-crystal value of 2.13 quoted in Refs. [14,15].

The values for *pe* and *papa* orientations are similar for all samples except HBN, where the *pe* value is slightly lower. The

Table 2
Refractive indices and loss coefficients of the four grades of *h*-BN studied.

	Refractive index @ 1 THz ± 0.002				Refractive index @ 2 THz ± 0.002				Loss @ 2 THz (cm^{-1}) ± 2%		
	pe	*papa*	*pape*	$n_e - n_o$	*pe*	*papa*	*pape*	$n_e - n_o$	*pe*	*papa*	*pape*
HBN	2.075	2.085	2.197	−0.112	2.075	2.087	2.197	−0.110	1.95	2.41	2.15
HBR	2.004	2.005	2.134	−0.129	1.992	1.995	2.128	−0.133	10.0	10.9	10.9
HBC	2.053	2.053	2.197	−0.144	2.057	2.058	2.2	−0.142	3.36	3.03	2.59
HBT	2.005	2.005	2.196	−0.191	2.015	2.015	2.202	−0.187	13.0	13.1	5.19

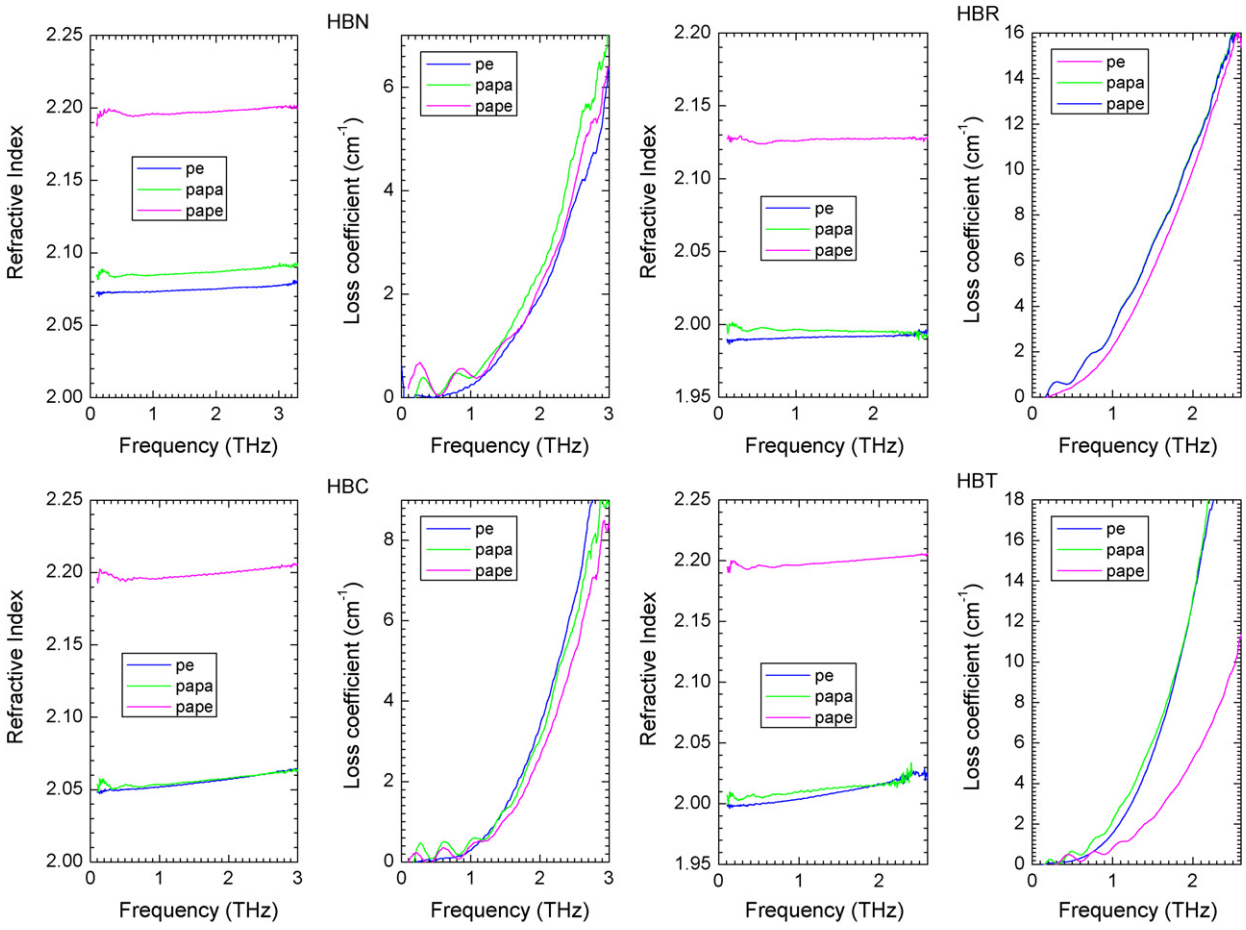

Fig. 4. THz refractive indices and loss coefficients of the four grades of *h*-BN studied. Sample orientations are denoted as follows: *pe* = cut perpendicular to the pressing axis; *papa* = cut parallel to the pressing axis, placed parallel to the THz beam polarisation; *pape* = cut parallel to the pressing axis, placed perpendicular to the THz beam polarisation. Values for *pe* and *papa* orientations are expected to be similar.

HBN grade contains <5% B_2O_3, which in its glassy form has the refractive index of 1.75.[19,20] B_2O_3 is a glass former, and will vitrify under the hot-pressing process. Therefore the material structure is expected to be that of BN platelets bound by vitreous B_2O_3 "glue". The low-porosity of HBN also supports this view. Since the *c*-plane has low surface energy, which precludes chemical interactions, the binder "glue" is expected to be segregated at the edges of the *c*-planes. Therefore the transmitted THz beam would interact with a greater volume of binder in the *pe* than in the *papa* orientation, thus lowering the measured refractive index. This is because the beam cross-section is much larger than the sample thickness, so that more platelet edges are incorporated in the interaction volume of the beam in the *pe* orientation than in *papa*. Assuming a 4% content of vitreous B_2O_3 in the *pa* beam path, the resulting refractive index would be $2.085 \times 0.96 + 1.75 \times 0.05 = 2.072$, which is close to the observed value of 2.075.

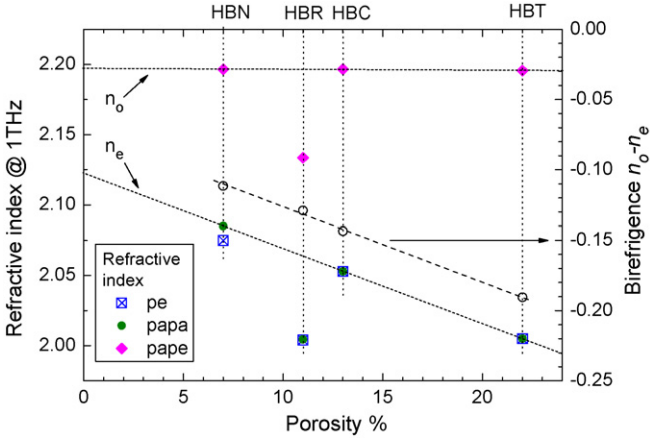

Fig. 5. Refractive index of the four *h*-BN grades studied at 1 THz, together with their birefringence.

The HBR grade has lower values of refractive index than expected for its porosity, although its birefringence complies with the trend. HBR contains ~6% of $Ca_3(BO_3)_2$ as binder. It may be speculated that $Ca_3(BO_3)_2$ – which unlike B_2O_3 is not a glass-former – donates oxygen to BN to form a variety of boron-oxide, boron-nitrogen-oxide and calcium-nitrogen-oxide compounds.[21] If these have lower refractive indices than BN, this would explain the observed low values in the HBR samples (regrettably, no data could be found in the literature). In addition, such compounds may also have higher densities, thus skewing the calculated porosity to incorrectly lower values. However, the fact that its ordinary refractive index is also significantly lower, and that its birefringence follows the trend of other grades, sug-

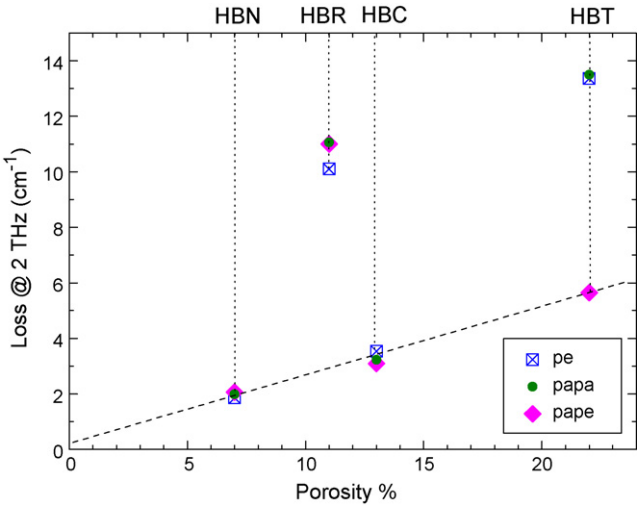

Fig. 6. Loss at 2 THz of the four *h*-BN grades studied.

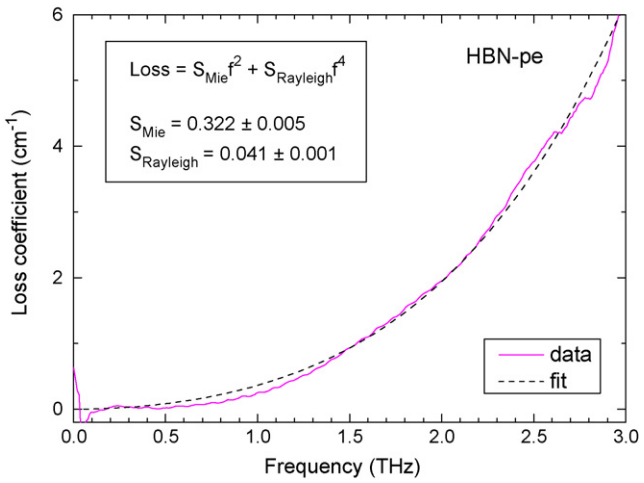

Fig. 7. The loss spectrum of HBN-*pe* together with the fit to the scattering model.

gests that any errors in HBR porosity are likely to be relatively small.

Fig. 6 depicts the relationship between loss and porosity. In ceramic materials loss is caused by combined contributions of absorption and scattering. If absorption is the dominant mechanism, then samples with higher porosity will have reduced losses because less material lies in the beam path. Conversely, if scattering predominates, then loss will rise with porosity due to the greater presence of scattering centres. As Fig. 6 shows, among the four grades of BN studied, loss increases with porosity, indicating that scattering is the dominant cause (see discussion below).

As expected, the losses in the *pe* and *papa* orientations are similar. Notably, the loss in the *pape* orientation rises linearly with porosity, and the value extrapolated to fully dense (zero porosity) is close to zero. This indicates that THz absorption in BN is very low, in agreement with data presented in Ref. [1].

In the HBT grade, losses in the *pe* and *papa* orientations are much higher than in *pape*. This is consistent with the view that porosity is segregated at the edges of the platelets, thus causing greater scattering of the beam polarised in the *ab*-plane. This is because for all angles of incidence s-polarised beam undergoes stronger reflection at interfaces, and therefore more scattering, than p-polarised beam.[22]

The HBR grade exhibits higher than expected loss. In the discussion above, it was speculated that HBR may contain a significant fraction of compounds incorporating Ca, O, N, and B. All such compounds are polar to a much greater degree than BN, and therefore highly absorbing at THz frequencies, giving rise to absorption losses. Moreover, grains of calcium-containing compounds are known to approach 100 μm in size,[23] causing greatly increased scattering from interfaces. Higher than calculated values of porosity would also contribute to increased scattering.

Scattering loss is frequency dependent; the nature of the dependence indicates the size of the scatterers. When scatterers are of the order of the wavelength and of varying sizes and shapes (Mie), the loss is proportional to f^2; when scatterers are much smaller than the wavelength (Rayleigh), the loss is proportional to f^4 [22] (where f is the frequency of the propagating radiation).

The loss spectra of the samples have been fitted with the scattering model, as shown in Fig. 7, using the equation:

$$\text{Loss} = S_{Mie}\, f^2 + S_{Rayleigh}\ \ f^4 \tag{3}$$

The ratio of the two scattering coefficients $S_{Mie}f^2/S_{Rayleigh}f^4$ may be taken to represent the relative predominance of scatterers of different sizes, and is plotted in Fig. 8.

It is seen that in all grades and orientations the ratio $S_{Mie}f^2/S_{Rayleigh}f^4 > 1$, signaling that the f^2 scattering is the dominant mechanism. This suggests that a significant proportion of the scatterers are of the order of >10 μm. Indeed, the HBR grade showed only f^2 scattering, marking the absence of small scatterers. This is consistent with the known size of calcium-compound grains in the material, which are known to be of the order of ~100 μm.[23] The ratio of scattering coefficients was significantly higher for the *pape* orientation than for *pe* or *papa*, which sup-

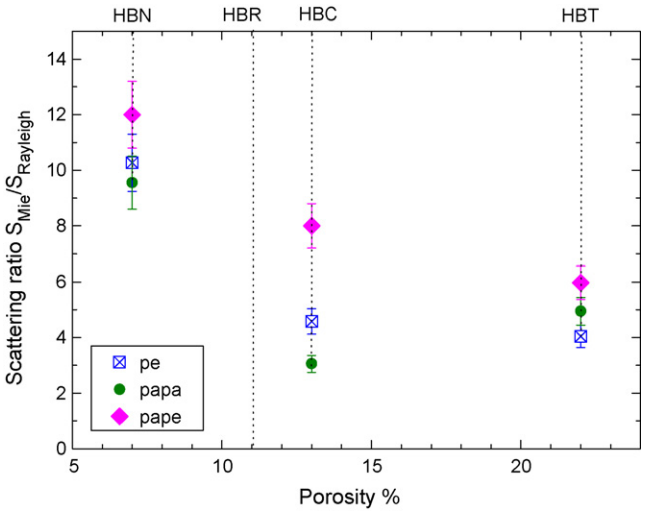

Fig. 8. The ratio of scattering coefficients $S_{Mie}f^2/S_{Rayleigh}f^4$ for HBN, HBC and HBT grades. The HBR grade had $S_{Rayleigh}f^4 \sim 0$ in all orientations.

ports the view that in this orientation the beam interacts with the edges of relatively large platelets. Notably, the ratio decreases with porosity, indicating that in more porous material the size of particles and pores may be smaller than in more highly dense material.

5. Conclusions

Four grades of *h*-BN were studied using THz time-domain spectroscopy. Significant differences were observed among the four grades in terms of their refractive indices and transmission loss. The results were analysed in relation to variations in porosity, composition and structure of the materials.

In particular, the analysis confirmed that both porosity and binder tend to be segregated at *c*-plane edges of the BN platelets. An indication of the sizes of particles and pores was also obtained.

THz time-domain spectroscopy was demonstrated as a technique capable of providing insight into the structure of optically opaque ceramic materials.

The low-porosity HBN grade was shown to have good transparency at THz frequencies. Moreover, the results indicate that by reducing porosity further, transparency can be greatly improved. However, when selecting the appropriate material for an application, one must consider the slightly lower loss in HBN versus the lack of moisture sensitivity in HBC. Both HBN and HBC grades have potential uses as optical materials at THz frequencies, especially in applications requiring high thermal resistance and/or hardness.

Acknowledgements

The work at the National Physical Laboratory was supported by the 2006–2009 Physical Programme of the National Measurement Office, an Executive Agency of the UK Department for Business, Innovation and Skills. The authors are grateful to Momentive Performance Materials for the provision of boron nitride samples.

References

1. Geick R, Perry CH, Rupprecht G. Normal modes in hexagonal boron nitride. *Phys Rev* 1966;**146**(2):543–7.
2. http://www.ioffe.rssi.ru/SVA/NSM/Semicond/BN/basic.html.
3. Bundy FP, Wentorf RH. Direct transformation of hexagonal boron nitride to denser forms. *J Chem Phys* 1963;**38**(5):1144–9.
4. Wentorf RH. Synthesis of the cubic form of boron nitride. *J Chem Phys* 1961;**34**(3):809–12.
5. Kimura Y, Wakabayashi T, Okada K, Wada T, Nishikawa H. Boron nitride as a lubricant additive. *Wear* 1999;**232**(2):199–206.
6. Yi G, Yan F. Effect of hexagonal boron nitride and calcined petroleum coke on friction and wear behavior of phenolic resin-based friction composites. *Mater Sci Eng A* 2006;**425**:330–8.
7. Mariani G. Selection and application of solid lubricants as friction modifiers. In: Rudnick L, editor. *Lubricant additives—chemistry and applications*. Boca Raton, FL: CRC Press, Taylor & Francis Group; 2003. p. 180–2.
8. J. Leist, M. Sinha, R. Rojas-Wahl, Optical Properties of Sensory Enhancers in a Simple Moisturizer Cream, to be presented at the New York Society of Cosmetic Chemists (NY-SCC) Technology Showcase, Dec. 2010.
9. Rudolph S. Composition and application of coatings based on boron nitride. *Interceram* 1993;**42**(5):302–5.
10. Raman C, Meneghetti P. Boron nitride finds new applications in thermoplastic compounds. *Plast Addit Compd* 2008;**10**(3):26–31.
11. Faraoun HI, Grosdidier T, Seichepine J-L, Goran D, Auorag H, Coddet C, et al. Improvement of thermally sprayed abradable coating by microstructure control. *Surf Coat Technol* 2006;**201**:2303–12.
12. Wu H, Zhang W. Fabrication and properties of ZrB_2–SiC–BN machinable ceramics. *J Eur Ceram Soc* 2010;**30**:1035–42.
13. Gatesman AJ, Giles RH, Waldman J. Submillimeter optical properties of hexagonal boron nitride. *J Appl Phys* 1993;**73**:3962–6.
14. Ishii T, Sato T. Growth of single crystals of hexagonal boron nitride. *J Cryst Growth* 1983;**61**:689–90.
15. Gielisse PJ, Mitra SS, Plendl JN, Griffis RD, Mansur LC, Marshall R, et al. Lattice infrared spectra of boron nitride and boron monophosphide. *Phys Rev* 1967;**155**(3):1039–46.
16. Rusanova LN, Gorchakova LI. Sintering of turbostratic-structure boron nitride powders. *Powder Met Met Ceram* 1989;**28**(2):108–11.
17. Beard MC, Turner GM, Schmuttenmaer CA. Terahertz spectroscopy. *J Phys Chem* 2002;**106**:1746–7159.
18. Hoffman DM, Doll GL, Eklund PC. Optical properties of pyrolytic boron nitride in the energy range 0.05–10 eV. *Phys Rev B* 1984;**30**(10): 6051–6.
19. Galeener FL, Lucovsky G, Mikkelsen Jr JC. Vibrational spectra and the structure of pure vitreous B_2O_3. *Phys Rev B* 1980;**22**(8):3983–90.
20. Verhoef AH, den Hartog HW. Infrared spectroscopy of network and cation dynamics in binary and mixed alkali borate glasses. *J Non-Cryst Solids* 1995;**182**:221–34.
21. Camurlu HE, Sevinc N, Topkaya Y. Effect of calcium carbonate addition on carbothermic formation of hexagonal boron nitride. *J Eur Ceram Soc* 2008;**28**:679–89.
22. Born M, Wolf E. *Principles of optics*. 6th ed. Pergamon Press; 1980.
23. Data proprietary to Momentive Performance Materials.